IEEE Access
Multidisciplinary | Rapid Review | Open Access Journal

Received June 25, 2019, accepted June 28, 2019, date of publication July 9, 2019, date of current version July 31, 2019.

Digital Object Identifier 10.1109/ACCESS.2019.2927537

Design and Analysis of a Novel Bearingless Segmented Switched Reluctance Motor

YONGHONG HUANG, FENGXIAO HUANG, YE YUAN, FAN YANG, AND KAI XIE
School of Electrical and Information Engineering, Jiangsu University, Zhenjiang 212013, China

Corresponding author: Yonghong Huang (hyh@ujs.edu.cn)

This work was supported in part by the National Natural Science Foundation of China under Project 51707082 and Project 51877101, in part by the Natural Science Foundation of Jiangsu Province of China under Grant BK20170546, and in part by the Priority Academic Program Development of Jiangsu Higher Education Institutions (PAPD).

ABSTRACT A novel bearingless segmented switched reluctance motor (BSSRM) is proposed in this paper to solve the coupling problem of the traditional bearingless switched reluctance motor (BSRM). Different from traditional BSRMs, the proposed BSSRM adopts the double stator and segmented rotor structure, thereby making the motor operate in short flux paths and the magnetic flux path isolated between torque and suspension system. On the basis of introducing the structure and working principle of the BSSRM, the mathematical model of torque and suspension force is deduced. The 2D finite element simulation model is established by the Ansoft software. The influence of structural parameters on torque and suspension system is analyzed, and its electromagnetic characteristic and decoupling characteristic are analyzed. Compared with the double stator bearingless switched reluctance motor (DSBSRM), the BSSRM not only improves the torque and suspension output but also weakens the coupling between torque and suspension system. Finally, the simulation results verify the effectiveness of the BSSRM.

INDEX TERMS Bearingless switched reluctance motor, segmented rotor, decoupling characteristic, electromagnetic characteristic.

I. INTRODUCTION

Bearingless switched reluctance motor (BSRM) not only inherits high-speed performance and adaptability to harsh environment of SRMs, but also takes advantages of magnetic bearing with low loss and no friction [1]–[4]. It can be promoted in various practical industrial applications, such as flywheel energy storage system, electric vehicle, aerospace and other fields [5]–[8].

The suspension and torque windings of the traditional BSRM show a nonlinear strong coupling relationship, which makes motor control complex and difficult [9]–[12]. Recent years, some scholars try to weaken the coupling between windings from the perspective of motor structure, and carry out researches on novel BSRMs [13]–[19]. In references [13], [14], an 8/10 hybrid stator BSRM is proposed. The stator teeth are composed of two types, with wide stator teeth for controlling suspension and narrow stator teeth for providing torque, which reduces the coupling between torque and suspension force. However, it causes the problems such as long torque magnetic path and reverse flux of stator yoke. On this basis, a 12/14 hybrid stator BSRM [15], [16] is proposed by Professor J. Ahn, which combines two adjacent torque poles to achieve short magnetic path characteristics of torque. But there are still disadvantages such as small commutation torque and low power density. In reference [17], the BSRM with wide rotor divides inductance region into suspension and torque regions, thereby achieving the decoupling of the torque and suspension. But its non-conducting phase still has magnetic flux, and the motor has low operating efficiency. Reference [18] proposed a double stator bearingless switched reluctance motor (DSBSRM), which the suspension and torque windings are respectively wound on the inner and outer stators. It can effectively overcome the coupling between suspension and torque compared with the hybrid stator BSRM.

The rotor of segmented SRM (SSRM) is constructed from a series of discrete segments, in which the segmental core is embedded in aluminum rotor block in order to improve the torque performance [20], [21]. To further weaken the coupling between torque and suspension system, and improve torque and suspension output capability, a novel bearingless

The associate editor coordinating the review of this manuscript and approving it for publication was Giambattista Gruosso.

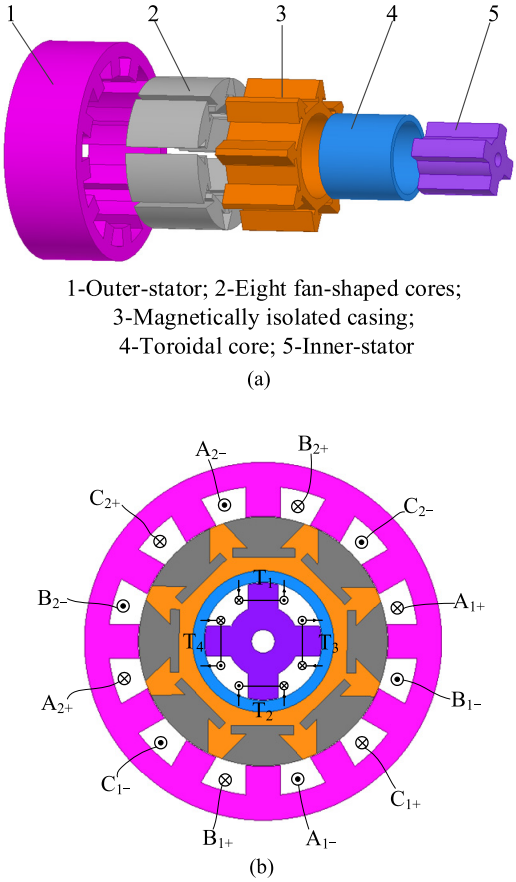

FIGURE 1. Model of the BSSRM. (a) 3D-model. (b) Cross section.

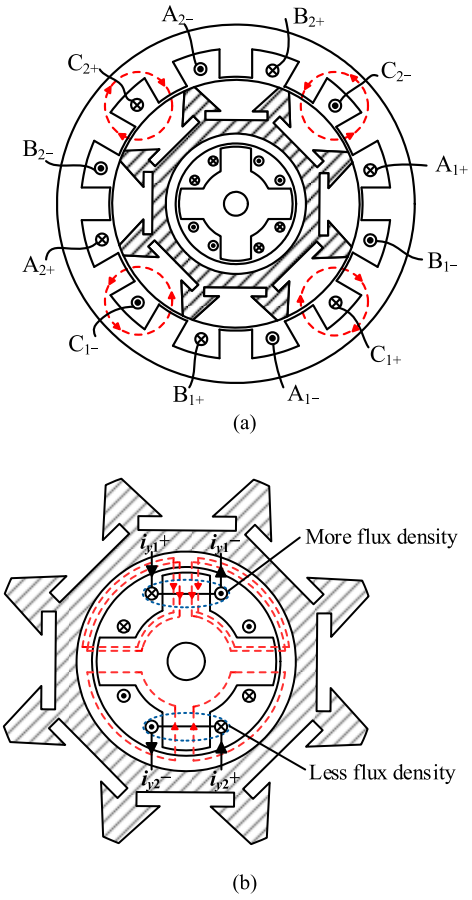

FIGURE 2. Operation principle of the BSSRM. (a) Torque. (b) Suspension force.

segmented switched reluctance motor (BSSRM) is proposed, which combines the excellent characteristics of SSRM and DSBSRM.

In this paper, the structure and working principle of BSSRM are introduced, and the mathematical model of torque and suspension force is deduced. Finite element method (FEM) is employed to establish the 2D-model of BSSRM and determine some important parameters affecting torque and suspension performance. Its electromagnetic characteristic and decoupling characteristic are analyzed. Compared with the traditional DSBSRM, the BSSRM has a great improvement of self-decoupling performance in the torque and suspension system. And it can obtain higher torque and suspension output.

II. TOPOLOGY AND OPERATING PRINCIPLE OF BSSRM

A. TOPOLOGY

As shown in the Fig. 1, the proposed BSSRM is composed of an outer-stator with 12 poles, a rotor, an inner-stator with 4 poles and control windings. The rotor adopts a non-salient pole structure, which mainly consists of eight fan-shaped cores, a magnetically isolated casing and a toroidal core. The outer-stator has three-phase fully pitched windings to produce rotational torque. For instance, torque windings A_{1+}, A_{1-}, A_{2+}, A_{2-} all need to be wound across three outer-stator teeth, thus connected in series to construct phase A. Phases B and C are the same as phase A in the winding structure and the connection mode, and are located at 30° and 60° respectively in the counterclockwise direction of the phase A in the spatial position. Concentrated windings T_1, T_2, T_3 and T_4 are wrapped around the inner-stator poles to provide suspension force. These suspension windings need to be independently controlled.

B. OPERATION PRINCIPLE

The torque of BSSRM is generated by the outer-stator and eight fan-shaped cores of the rotor, as shown in Fig. 2(a). The rotating principle of BSSRM is similar to traditional SRMs, following the Minimum Principle of Reluctance. Due to the segmented rotor, its torque flux travels in a short flux loop, in contrast to traditional SRMs that use long flux loops.

Fig.2(b) shows the principle of suspension force production. Taking y direction as an example, suspension windings T_1, T_2 are applied with different currents. When the current i_{y1} is larger than i_{y2}, the magnetic flux density of air gap near winding T_1 is certainly greater than that of air gap near winding T_2. Due to the uneven magnetic flux density, suspension force in y positive direction is generated. In the same way, suspension force in x direction can also be generated.

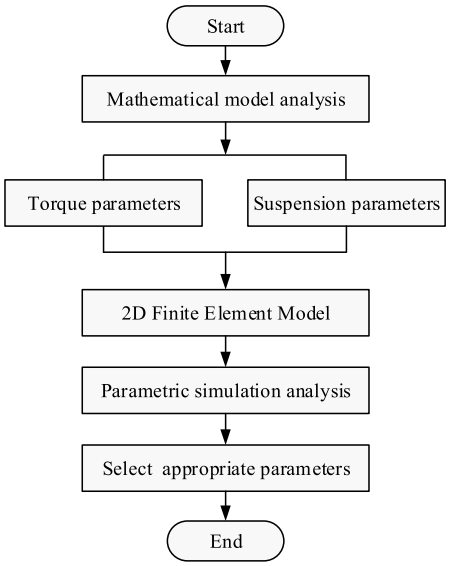

FIGURE 3. The specific flow chart.

The suspension force can be composed in any direction by suspension forces in x and y direction to meet the suspension requirements of the rotor.

III. MOTOR DESIGN

In order to achieve better torque and suspension performance of the motor, it is necessary to select the appropriate structural parameters. Based on the mathematical model of torque and suspension force, the influence of structural parameters on torque and suspension performance is analyzed. The finite element software is used to establish the 2D-model for parametric analysis. The specific flow chart is shown in Fig.3.

A. MATHEMATICAL MODEL

The working process of BSSRM is severely nonlinear, the same as the traditional SRM. It is impossible to strictly list the specific expressions of phase inductance and phase current. Therefore, the phase current and phase inductance of BSSRM are estimated empirically, that is, the winding current waveform is equivalent to a square wave. This estimation method is ignoring the effects of magnetic saturation and mutual inductance. Then the electromagnetic torque ($T_{\rm ph}$) of each phase can be expressed as follows

$$T_{ph} = \int \frac{1}{2}[i(\theta)]^2 \frac{\partial L(i,\theta)}{\partial \theta} \approx \frac{1}{2} I_{ph}^2 \frac{\Delta L}{\Delta \theta} \tag{1}$$

$$I = \sqrt{\frac{1}{T}\int_0^{T/2} I_{ph}^2 dt} = \frac{\sqrt{2}}{2} I_{ph} = k_i i_m \tag{2}$$

$$\Delta\theta \approx \theta_r/2 = \pi/Z_r \tag{3}$$

$$\Delta L = L_{\max} - L_{\min} = L_{\max}(1 - k_m) \tag{4}$$

where $I_{\rm ph}$ is the half-cycle average of the phase current; I is the effective value of the winding phase current; $i_{\rm m}$ is the peak value of the winding phase current; T is the period of the phase current;$L_{\max}$ and $L_{\min}$ are the phase maximum and minimum inductance; $Z_{\rm r}$ is the number of rotor teeth; $k_{\rm i}$ is the peak current coefficient, that is, the ratio of the effective value of the phase current to the peak value, generally taking $k_{\rm i} = 0.5$; $k_{\rm m}$ is the ratio of the phase minimum inductance to the maximum inductance.

Assuming that the eccentricity of rotor in the positive direction of x-axis and y-axis is x_0 and y_0 respectively, F_{x1}, F_{x2}, F_{y1} and F_{y2} are the suspension forces along the positive and negative directions of x-axis and y-axis, respectively, and can be expressed as

$$\begin{cases} F_{x1} = \dfrac{\mu_0 N_x^2 A}{2\,(g_2 - x_0)^2} i_{x1}^2 \\ F_{x2} = \dfrac{\mu_0 N_x^2 A}{2\,(g_2 + x_0)^2} i_{x2}^2 \\ F_{y1} = \dfrac{\mu_0 N_y^2 A}{2\,(g_2 - y_0)^2} i_{y1}^2 \\ F_{y2} = \dfrac{\mu_0 N_y^2 A}{2\,(g_2 + y_0)^2} i_{y2}^2 \end{cases} \tag{5}$$

where μ_0 is the air permeability in vacuum; g_2 is the length of suspension air gap; A is the pole area of the inner-stator; N_x and N_y are the turns of the suspension winding in x, y direction, respectively. i_{x1}, i_{x2}, i_{y1} and i_{y2} are suspension currents in the positive and negative directions of x-axis and y-axis, respectively.

B. AIR GAP SELECTION

Air gap is an important parameter that directly affects torque and suspension force of BSSRM. Ignoring the magnetic flux leakage, the torque air gap permeability of the maximum phase inductance ($\Lambda_{\max}$) can be expressed as follows

$$\Lambda_{\max} = \frac{\mu_0 L k_c}{2g_1}\left[\frac{\pi D \alpha_r}{Z_r} - \frac{\pi D(1-\alpha_s)}{Z_s}\right] \tag{6}$$

And the phase maximum inductance $L_{\max}$ be expressed

$$L_{\max} = \frac{Z_s N^2 \Lambda_{\max}}{2m} \tag{7}$$

where g_1 is the length of torque air gap; L is the thickness of the outer-stator; $k_{\rm c}$ is the lamination coefficient; D is the inner diameter of the outer-stator; $Z_{\rm s}$ is the number of the outer-stator teeth; N is the turns of the torque winding; m is the number of phases; $\alpha_{\rm r}$ and $\alpha_{\rm s}$ are the outer-stator and rotor pole arc coefficient, respectively.

From equations (1), (4), (6) and (7), the expression of $T_{\rm ph}$ and g_1 can be derived. And it can be found that the torque is inversely proportional to g_1. From equation (5), the suspension force is inversely proportional to the square of g_2. Fig. 4 presents the relationships between the torque and g_1, the suspension force and g_2.

It can be found that both torque-g_1, suspension force-g_2 are the decreasing function. Considering that the choice of air gaps should meet the requirements of machining, $g_1 = 0.3$mm and $g_2 = 0.3$mm are selected.

C. POLE ARCS SELECTION

The stator and rotor pole arcs have an influence on the static performance of BSSRM. FEM is used to get parameter values

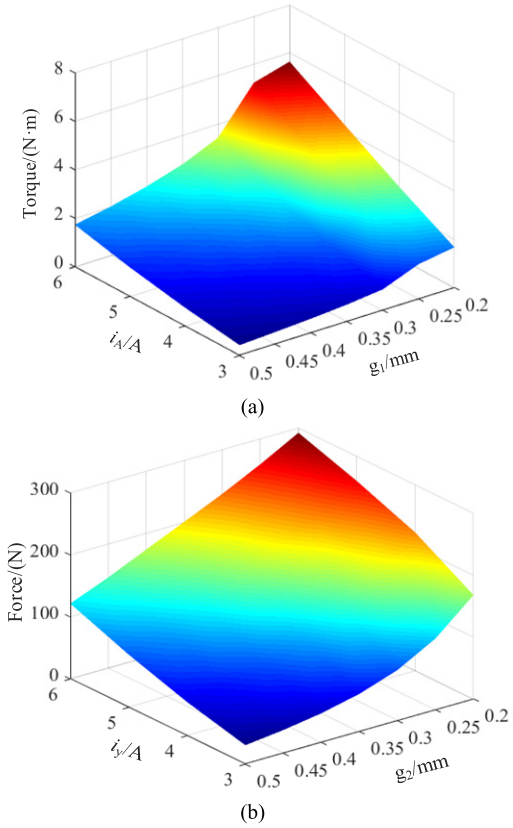

FIGURE 4. Torque performance and suspension performance of BSSRM. (a) The relationship between torque and g_1. (b) The relationship between suspension force and g_2.

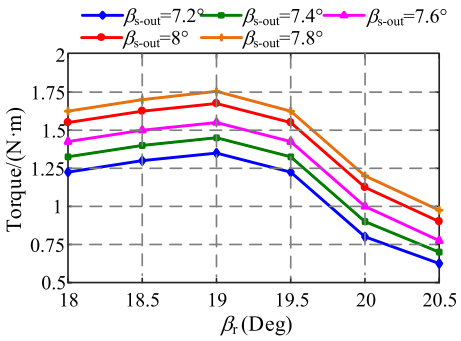

FIGURE 5. Relations between torque and rotor pole arc at different outer-stator pole arcs.

to ensure torque and suspension performance, where β_{s-out}, β_{s-in} and β_r are the outer-stator pole arc, the inner-stator pole arc and the rotor pole arc, respectively.

Fig.5 describes the variation of torque with the rotor pole arcs (β_r) at different outer-stator pole arcs (β_{s-out}). It should be noted that with the increase of β_r and β_{s-out}, the torque values increase first and then decrease. It is obvious that when $\beta_{s-out} = 7.8°$ and $\beta_r = 19°$, good torque performance can be obtained.

Fig.6 reveals the variation of suspension force with annular silicon steel sheet thicknesses (h_s) at different inner-stator

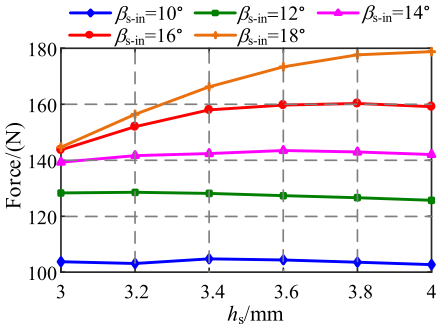

FIGURE 6. Relations between suspension force and annular silicon steel sheet thickness at different inner-stator pole arcs.

TABLE 1. Dimensions of the BSSRM.

Parameters	Value
Outer-stator outer diameter, inner diameter(mm)	120, 84
Inner-stator outer diameter, inner diameter(mm)	39.4, 8
Outer-stator yoke thickness(mm)	10
Rotor diameter(mm)	83
Airgap1,2 length(mm)	0.3, 0.3
Rotor yoke thickness(mm)	3.8
Rotor pole arc(deg)	19
Outer-stator, inner diameter pole arc(deg)	7.8, 15
Inner-stator yoke thickness(mm)	8
Turns of torque winding, suspension winding	80, 50

pole arcs (β_{s-in}). h_s has little effect on suspension force when β_{s-in} is in the range of 10° and 14°. While it is greater than 14°, the suspension force first increases and then remains stable with h_s, which is mainly due to the magnetic saturation phenomenon. It also can be observed that the suspension force and inner-stator pole arc are in an increasing relationship. So $\beta_{s-in} = 15°$, $h_s = 3.8$mm are selected.

IV. PERFORMANCE ANALYSIS

In order to study the performance of BSSRM, the 2D-model is established by using Ansoft software. In this section, characteristics, including inductance, torque, suspension force and decoupling, are analyzed. To further verify the excellent performance of BSSRM, the electromagnetic and decoupling performance of DSBSRM are compared. The parameters of BSSRM are listed in Table 1.

A. TORQUE CHARACTERISTICS

Fig.7 describes the magnetic density distribution of the rotor in an aligned position and a misaligned position when $i_{TA} = 4$A, where i_{TA} is the torque current of phase A. It can be seen that the torque magnetic flux is mainly concentrated in the phase A torque pole and corresponding sector-shaped rotor core, without passing through the magnetic isolation rotor sleeve and inner-stator. The magnetic flux density in an aligned position and a misaligned position are approximately 0.7T and 0.4T.

The inductance characteristic curve is shown in Fig.8, which i_{TA} varying from 3A to 6A. It can be obviously seen that for the three-phase BSSRM, the inductance values

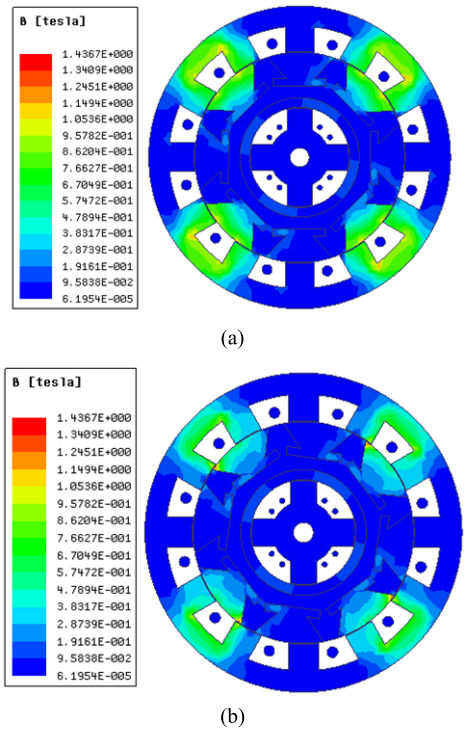

FIGURE 7. Magnetic density distribution with the torque current. (a). In an aligned position. (b). In a misaligned position.

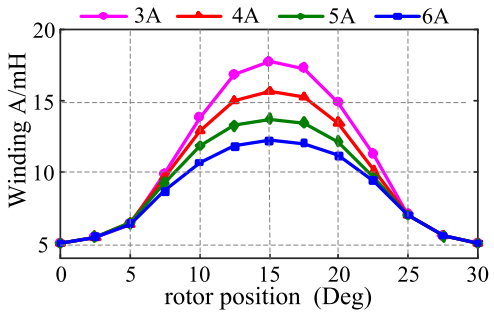

FIGURE 8. Inductance characteristic curve.

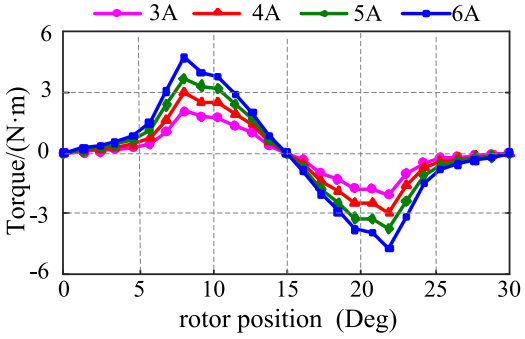

FIGURE 9. Torque values of the BSSRM.

increase first and then decrease with the rotor angle. It is evident that the inductance period is 30° and is symmetric about 15°.

Fig.9 depicts the torque versus rotor angular position for different phase current values. The torque current values are taken as 3A, 4A, 5A and 6A. The torque value is positive in the range of 0°-15°, while negative in the rotor position angle 15° to 30°. The torque curve has a symmetry that is at the rotor position angle 15°. In the range of 0°-15°, the graph shows that the torque values gradually increase till 8° and then decrease. From the graphical analysis it is concluded that, when the edge of the rotor pole coincides with the outer-stator teeth pole at all angles of rotor, the torque produced will be maximum, which matches the principle of minimum reluctance.

B. SUSPENSION CHARACTERISTICS

When the suspension current is applied alone in x positive direction ($i_x1 = 4$A), the magnetic density distribution and flux flow are shown in Fig.10 (a) and (b). It can be found that the suspension magnetic flux is mainly concentrated in the inner-stator suspension poles and rotor annular core, without passing through the outer-stator and sector-shaped rotor cores.

Fig.10 (c) shows the values of suspension force when the rotor rotates at a 2π angle. The suspension forces are approximately 30N, 55N, 83N, and 118N when 3A, 4A, 5A, and 6A suspension currents are applied in x positive direction, respectively. The suspension force in x direction increases linearly with the suspension current increasing. And it can be seen that suspension force remains unchanged when the rotor angular position changes.

As shown in Fig.10 (d), the suspension forces generated in y direction are approximately 0.85N, 1.2N, 2.2N, and 3N, which can be neglected compared with the suspension force generated in x direction. Therefore, the proposed motor can offer good suspension force performance.

C. DECOUPLING CHARACTERISTICS

Fig.11 (a) shows the magnetic flux density distribution when torque and suspension windings are energized concurrently. And it can be observed that the magnetic flux paths of the torque and suspension are independent from each other.

Fig.11 (b) presents the values of torque with different suspension currents (3A, 4A, 5A, 6A) while $i_{TA} = 0$A. From the figure, it is clear that by changing suspension currents there is very small change on torque. The maximum torque is less than 150nN·m. Therefore, the suspension current has almost no effect on torque.

Fig.11 (c) and (d) illustrates the values of suspension force in x and y direction when i_{TA} varies from 3A to 6A. The maximum suspension force is less than 2μN with torque current increases. From the above analysis it may be concluded that the coupling of torque and suspension force can be neglected.

D. COMPARISON OF CHARACTERISTICS

In order to further verify the excellent performance of BSSRM, the electromagnetic performance and decoupling performance of DSBSRM are compared. Both DSBSRM and BSSRM use the same dimension and input parameters.

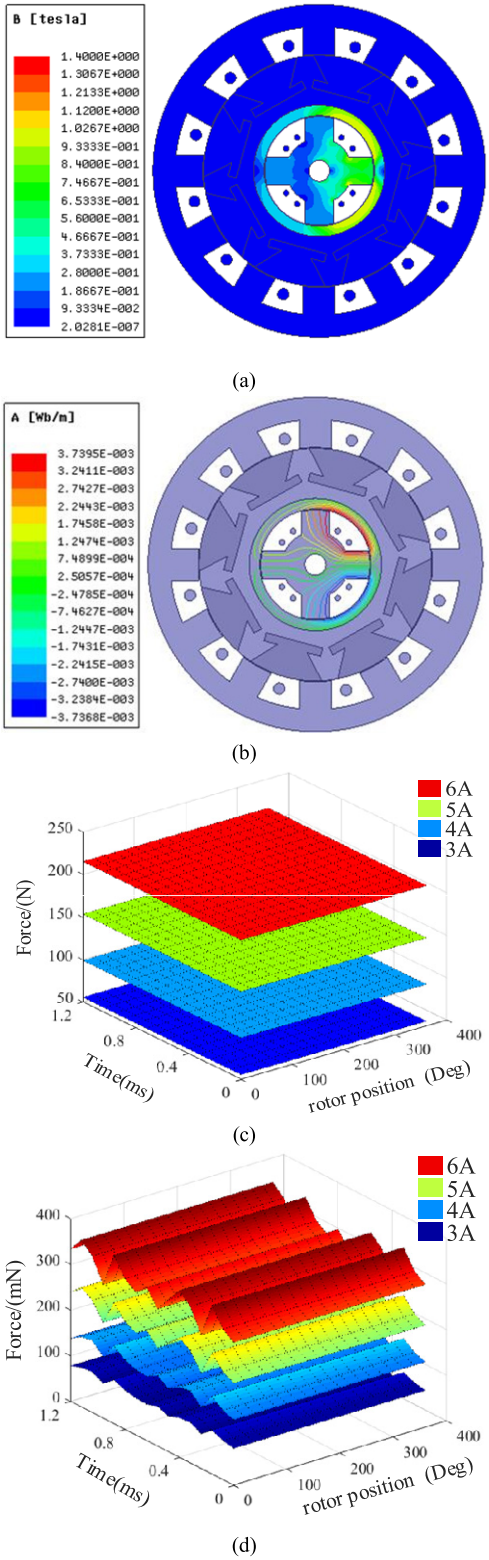

FIGURE 10. Suspension characteristic of the BSSRM. (a). Magnetic density distribution with the suspension current in *x* direction. (b). Flux flow with the suspension current in *x* direction. (c). Values of suspension force in *x* direction. (d). Values of suspension force in *y* direction.

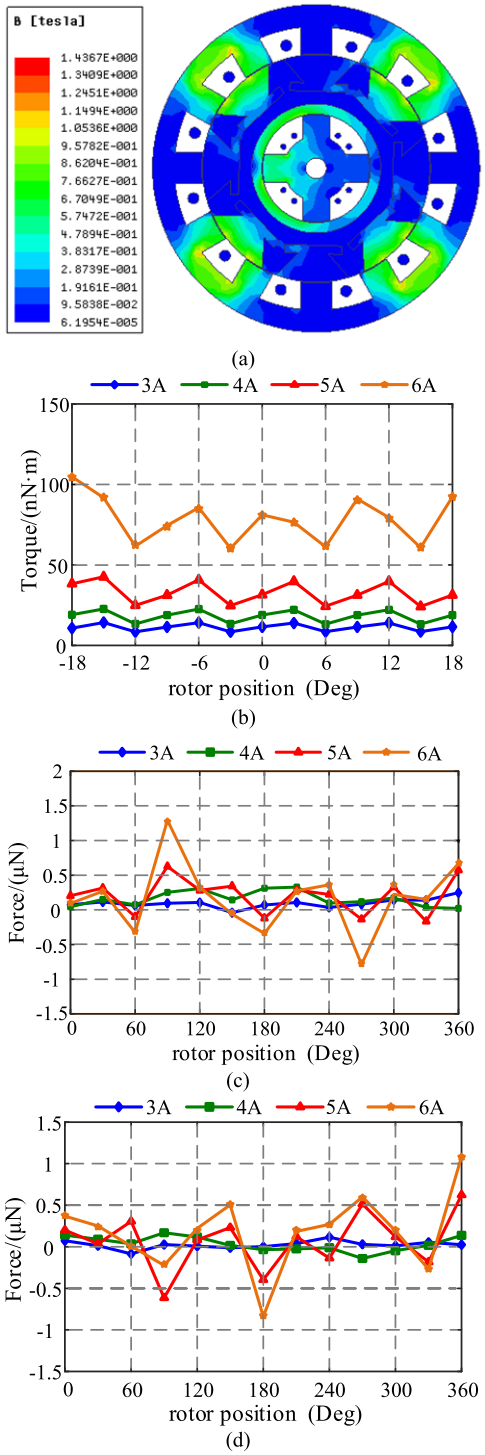

FIGURE 11. Decoupling characteristic of the BSSRM. (a). Magnetic density distribution with suspension current in *x* direction and torque current of phase A. (b). Values of torque with different suspension currents. (c). Values of suspension force in *x* direction with different torque currents. (d). Values of suspension force in *y* direction with different torque currents.

Fig.12 shows the torque and suspension force comparison of DSBSRM and BSSRM. The torque and suspension windings are respectively applied to the same current (i_{TA} = 3A, i_x1 = 3A). From Fig.12 (a), it can be calculated that the average torque of DSBSRM is 1.6N·m, while proposed one is 2.4N·m. The average torque of BSSRM is 50% higher than

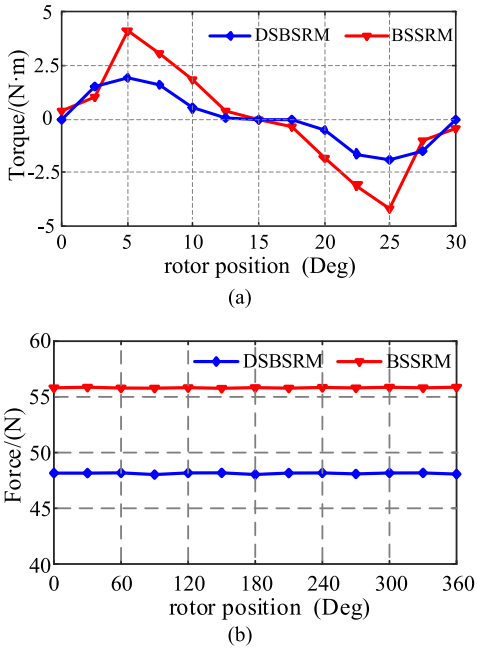

FIGURE 12. Comparison of the DSBSRM and BSSRM. (a). Torque. (b). Suspension force.

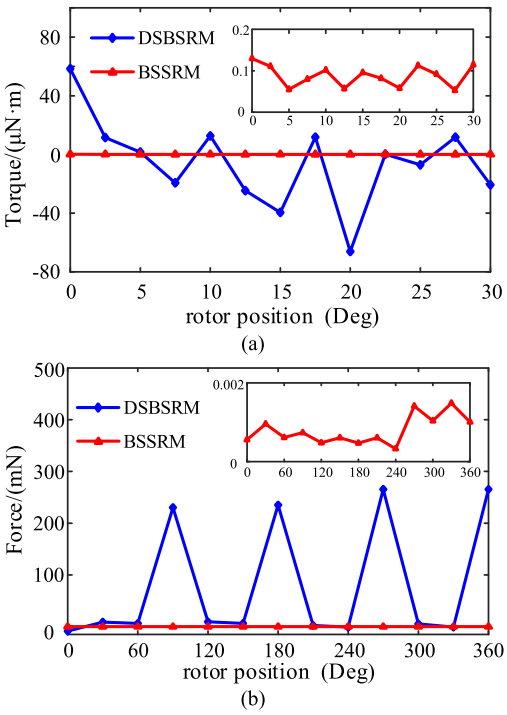

FIGURE 13. Decoupling comparison of the DSBSRM and BSSRM. (a). Torque. (b). Suspension force.

DSBSRM. It can be found from Fig.12 (b) that suspension force of BSSRM is 10N higher than DSBSRM. So BSSRM can provide higher torque and suspension force.

Fig.13 shows the decoupling characteristic comparison of DSBSRM and BSSRM. The torque and suspension windings are respectively applied to the same current (i_{TA} = 3A, i_x1 = 3A). As seen from the Fig.13 (a) and (b), the torque of BSSRM is less than 0.2μN·m, while the DSBSRM is 80μN·m. The suspension force of BSSRM is approximately 0.002mN, while DSBSRM is 300mN. Compared with DSBSRM, the torque and suspension force decoupling curves of BSSRM approximate a straight line with a value of 0, which can be neglected. The BSSRM has a great improvement of decoupling performance in torque and suspension system.

V. CONCLUSION

In this paper, a novel BSSRM is proposed, which adopts the double stator and segmented rotor structure, making the motor operate in short flux paths and the magnetic flux path isolated between torque and suspension system. The mathematical model of the torque and suspension force is deduced by introducing its structure and working principle. Then the 2D-model is established by Ansoft finite element software. The electromagnetic and decoupling characteristics are analyzed. A comparison between DSBSRM and BSSRM is also executed, which demonstrates that the BSSRM can offer better performance in term of torque/suspension output and self-decoupling between torque and suspension system. The motor parameters will be optimized and the prototype machine will be built in the future.

REFERENCES

[1] S. Yao and W. Zhang, "A simple strategy for parameters identification of SRM direct instantaneous torque control," *IEEE Trans. Power Electron.*, vol. 33, no. 4, pp. 3622–3630, Apr. 2018.

[2] Z. Djelloul-Khedda, K. Boughrara, F. Dubas, and R. Ibtiouen, "Nonlinear analytical prediction of magnetic field and electromagnetic performances in switched reluctance machines," *IEEE Trans. Magn.*, vol. 53, no. 7, Jul. 2017, Art. no. 8107311.

[3] L. Chen and W. Hofmann, "Speed regulation technique of one bearingless 8/6 switched reluctance motor with simpler single winding structure," *IEEE Trans. Ind. Electron.*, vol. 59, no. 6, pp. 2592–2600, Jun. 2012.

[4] J. Zhang, H. Wang, L. Chen, C. Tan, and Y. Wang, "Multi-objective optimal design of bearingless switched reluctance motor based on multi-objective genetic particle swarm optimizer," *IEEE Trans. Magn.*, vol. 54, no. 1, Jan. 2018, Art. no. 8100113.

[5] Y. Sun, Y. Yuan, and Y. Huang, "Design and analysis of bearingless flywheel motor specially for flywheel energy storage," *Electron. Lett.*, vol. 52, no. 1, pp. 66–68, 2016.

[6] D. Xingjian, J. Xinjian, W. Qiunan, W. Yong, and W. Shanming, "The design and testing of a 1 MW/60 MJ flywheel energy storage power system," *Trans. China Electrotechn. Soci.*, vol. 32, no. 21, pp. 89–95, Nov. 2017.

[7] C. Gan, J. Wu, Q. Sun, W. Kong, H. Li, and Y. Hu, "A review on machine topologies and control techniques for low-noise switched reluctance motors in electric vehicle applications," *IEEE Access*, vol. 6, pp. 31430–31443, 2018.

[8] Y. Sun, Y. Huang, and Y. Yuan, "Radial force dynamic current compensation method of single winding bearingless flywheel motor," *IET Power Electr.*, vol. 8, no. 7, pp. 1224–1229, 2015.

[9] X. Cao, H. Yang, L. Zhang, and Z. Deng, "Compensation strategy of levitation forces for single-winding bearingless switched reluctance motor with one winding total short circuited," *IEEE Trans. Ind. Electron.*, vol. 63, no. 9, pp. 5534–5546, Sep. 2016.

[10] Z. Zhu, Q. Wan, and Y. Sun, "An ELM identifier and inverse controller based algorithm for dynamic decoupling control of bearingless switched reluctance motor," in *Proc. 20th Int. Conf. Elect. Mach. Syst. (ICEMS)*, Aug. 2017, pp. 1–6. doi: 10.1109/ICEMS.2017.8056367.

[11] M. Dev Choudhury, F. Ahmed, G. Kumar, K. Kalita, and K. Tammi, "Design methodology for a special single winding based bearingless switched reluctance motor," *J. Eng.*, vol. 2017, no. 7, pp. 274–284, 2017.
[12] L. Chen, H. Wang, J. Zhang, C. Tan, and Y. Wang, "Coordinated control strategy based on adjustable turn-off angle for bearingless switched reluctance motor," in *Proc. 13th IEEE Conf. Ind. Electron. Appl. (ICIEA)*, Jun. 2018, pp. 724–729.
[13] Z. Y. Zhu, Y.-J. Jiang, J. Zhu, and X. Guo, "Performance comparison of 12/12 pole with 8/10 and 12/14 pole bearingless switched reluctance machine," *Electron. Lett.*, vol. 55, no. 6, pp. 327–329, Mar. 2019.
[14] H. Wang, Y. Wang, and J.-W. Ahn, "Design of novel bearingless switched reluctance motor," *IET Electr. Power Appl.*, vol. 6, no. 2, pp. 73–81, Feb. 2012.
[15] Z. Xu, D.-H. Lee, and J.-W. Ahn, "Comparative analysis of bearingless switched reluctance motors with decoupled suspending force control," *IEEE Trans. Ind. Appl.*, vol. 51, no. 1, pp. 733–743, Jan./Feb. 2015.
[16] H. Wang, S. Tang, and B. Xue, "New type 12/14 bearingless switched reluctance motor with double windings," *IET Electr. Power Appl.*, vol. 9, no. 7, pp. 478–485, Aug. 2015.
[17] Y. Yang, F. Liu, and C. Liu, "A new bearingless switched reluctance motor with wide rotor pole arc," in *Proc. 9th IEEE Conf. Ind. Electron. Appl. (ICIEA)*, Jun. 2014, pp. 374–378.
[18] W. Peng, D.-H. Lee, F. Zhang, and J.-W. Ahn, "Design and characteristic analysis of a novel bearingless SRM with double stator," in *Proc. Int. Conf. Elect. Mach. Syst.*, Aug. 2011, pp. 1–6. doi: 10.1109/ICEMS.2011.6073471.
[19] Y. Sun, F. Yang, Y. Yuan, F. Yu, Q. Xiang, and Z. Zhu, "Analysis of a hybrid double stator bearingless switched reluctance motor," *IET Electron. Lett.*, vol. 54, no. 24, pp. 1397–1399, Nov. 2018.
[20] Z. Xu, J. Liu, M.-J. Kim, D.-H. Lee, and J.-W. Ahn, "Characteristics analysis and comparison of conventional and segmental rotor type 12/8 switched reluctance motors," *IEEE Trans. Ind Appl.*, vol. 55, no. 3, pp. 3129–3137, May/Jun. 2019.
[21] R. Madhavan and B. G. Fernandes, "Performance improvement in the axial flux-segmented rotor-switched reluctance motor," *IEEE Trans. Energy Convers.*, vol. 29, no. 3, pp. 641–651, Sep. 2014.

YONGHONG HUANG received the M.Sc. degree in control theory and engineering and the Ph.D. degree in agricultural electrification and automation from Jiangsu University, Zhenjiang, China, in 1998 and 2009, respectively.

Her research interest includes motor control for new energy vehicle.

FENGXIAO HUANG received the B.Sc. degree in electrical engineering from Jiangsu University, Zhenjiang, China, in 2017, where she is currently pursuing the M.Sc. degree in electrical engineering.

Her current research interests include bearingless switched reluctance machine design and analysis.

YE YUAN received the M.Sc. degree in power electronics and power drives and the Ph.D. degree in electrical engineering from Jiangsu University, Zhenjiang, China, in 2011 and 2016, respectively.

His research interest includes bearingless motor design and control.

FAN YANG received the M.Sc. degree in electrical engineering from Jiangsu University, in 2015, where he is currently pursuing the Ph.D. degree in electrical engineering.

His research fields include motor design and control, and flywheel energy storage.

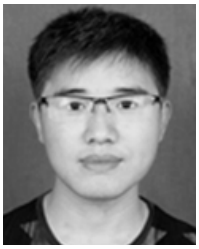

KAI XIE is currently pursuing the M.Sc. degree in electrical engineering.

His research interest includes bearingless motor control for flywheel energy storage.